frontiers in Materials

ORIGINAL RESEARCH
published: 31 March 2020
doi: 10.3389/fmats.2020.00057

Cr^{+6} Controlled Nucleation in SiO_2-MgO-Al_2O_3-K_2O-B_2O_3-F Glass Sealant (SOFC)

Mrinmoy Garai[1,2], Basudeb Karmakar[2] and Shibayan Roy[1]*

[1] Materials Science Centre, Indian Institute of Technology (IIT), Kharagpur, India, [2] Glass Science and Technology Section, CSIR-Central Glass & Ceramic Research Institute (CGCRI), Kolkata, India

This study highlights the strong effect of chromium (Cr^{6+}) as a nucleating agent for SiO_2-MgO-Al_2O_3-B_2O_3-K_2O-F glass sealant. In the process, Al_2O_3 from the base glass was gradually substituted by $K_2Cr_2O_7$, which considerably tuned the crystallization characteristics, microstructure, thermal, and mechanical properties. The distinctive feature of this study is the induction of nucleation and crystallization in glass matrix on addition of Cr^{6+} content performing only annealing heat-treatment (600°C). The melt-quenched SiO_2-MgO-Al_2O_3-B_2O_3-K_2O-F glass with zero Cr^{6+} content is found amorphous, which in presence of Cr^{6+} content became crystalline with $MgCr_2O_4$, K_3CrF_6, MgF_2, and mullite ($3Al_2O_3.2SiO_2$) phases. Glassy features in DSC and dilatometric thermal properties (T_g, T_d, thermal expansion) were attained in glass without Cr- content, but glass-ceramic-like features obtained for Cr- containing glasses. Large thermal expansion ($>11 \times 10^{-6}$/K) was achieved for such glasses, and that is compatible with the CTE of solid oxide fuel cell (SOFC) components (electrode, interconnect, etc.) at the operating temperature (700–900°C). FESEM study revealed the development of 200–500 nm sized crystallites in 2 mol% $K_2Cr_2O_7$-containing glass microstructure and that became more compact sorted with 10–50 μm sized crystals in higher Cr-doped glasses. Higher crystallinity was thus ascertained for higher Cr-containing glasses, which influenced the corresponding density and mechanical properties. From nano-indentation measurements, the hardness and Young's modulus were estimated to be 0.6 (±0.5) and 25 (±10) GPa, respectively, for base glass and in the range of 3.3 to 8.4 and 58 to 94 GPa, respectively, for Cr-containing glass-ceramics. Hardness measured from micro-indentation tests for the base glass was 3.63 (± 0.18) GPa, which increased to 3.94–6.08 GPa for Cr-containing glass-ceramics. Due to the typical microstructure and compatible thermal and mechanical properties, 2 mol% $K_2Cr_2O_7$-doped SiO_2-MgO-Al_2O_3-B_2O_3-K_2O-F glass can be useable as high temperature sealant (like SOFC).

Keywords: glass, crystallization - amorphous systems, microstructure, thermal expansion coefficient, microhardness, sealant, glass ceramic (MACOR)

OPEN ACCESS

Edited by:
Ana C. M. Rodrigues, Federal University of São Carlos, Brazil

Reviewed by:
Aluisio Alves Cabral Junior, Federal University of Maranhão, Ministry of Education, Brazil
Rafael Bianchini Nuernberg, CEA Marcoule, France

****Correspondence:***
Mrinmoy Garai
mrinmoygarai@iitkgp.ac.in;
mrinmoygarai@yahoo.in

Specialty section:
This article was submitted to Ceramics and Glass, a section of the journal Frontiers in Materials

Received: *19 October 2019*
Accepted: *26 February 2020*
Published: *31 March 2020*

Citation:
Garai M, Karmakar B and Roy S (2020) Cr^{+6} Controlled Nucleation in SiO_2-MgO-Al_2O_3-K_2O-B_2O_3-F Glass Sealant (SOFC). Front. Mater. 7:57. doi: 10.3389/fmats.2020.00057

INTRODUCTION

Since the development of glass-ceramics, alkaline earth ions containing borosilicate glasses have been a thrilling research area due to their typical microstructural characteristics after controlled heat treatment (Holand et al., 2001; Beall, 2014; Deubener and Höland, 2017; Lin et al., 2018). Because of significant advantages in physical, thermal, and mechanical properties after crystallization, these glasses is ideal for high temperature applications, such as solid oxide fuel cell (SOFC). K_2O-MgO-B_2O_3-SiO_2-F is one unique kind of borosilicate glass system, which is converted to glass-ceramic with huge microstructural amendments (Deubener and Höland, 2017). In common practice, a typical heat treatment schedule is followed for converting borosilicate glass to glass-ceramic (McDowell and Beall, 1969; Mcmillan, 1979; Pingale et al., 1996). Sometimes, external nucleating agents are added for better crystallization (Mcmillan, 1979). This kind of follow up makes the heat treatment schedule a crucial assignment in addition to the selection of a nucleating agent for the particular glass composition for attaining proper crystallization (McDowell and Beall, 1969; Mcmillan, 1979; Pingale et al., 1996; Deubener and Höland, 2017). The heat treatment requires both time and electrical energy. It is of the utmost desire to get the glass crystallized by putting in the least effort, and, if possible, without performing any heat treatment at all (McDowell and Beall, 1969; Deubener and Höland, 2017). For this purpose, self-nucleation during the glass melting or annealing is desired. However, it is obviously a tedious job.

Transition metal constituents like manganese, iron, cobalt, nickel, copper, chromium, molybdenum, and tungsten are well-known doping agents that are extensively used in the glass industry as coloring ions (McDowell and Beall, 1969; Mcmillan, 1979; Pingale et al., 1996; Deubener and Höland, 2017; Lin et al., 2018; Aktas et al., 2019). For chromium (Cr), being a multivalent ion when added to a glass batch as Cr_2O_3, $K_2Cr_2O_7$, or iron–magnesium–aluminum chromite such as $(Fe,Mg)O(Cr,Al)_2O_3$, the Cr^{3+}, Cr^{4+}, or Cr^{6+} are generally estimated (Pingale et al., 1996; Lin et al., 2018; Aktas et al., 2019). Chromium (Cr^{n+}) has strong ability to act variably in Si-O-B/Si-O-Al structure (glass) in different oxidation states (i.e., varying charge/radius) (Pingale et al., 1996; Aktas et al., 2019). Cr^{3+} serves as a modifier, whereas Cr^{6+}, in the form of CrO_4^{2-} structural units, can act as the glass network (Lin et al., 2018). Higher valence chromium ion (Cr^{n+}) affects the crystallization as well as microstructure in borosilicate glass (Shelby, 2005; Aktas et al., 2019). Having large cationic field strength, these transition metal ions [in particular, chromium (Cr^{n+}), molybdenum, and tungsten] can act as nucleation catalyst for initiating heterogeneous phase separation in Si-O-Si matrix (McDowell and Beall, 1969; Shelby, 2005). As a consequence of nucleation in K_2O-MgO-B_2O_3-SiO_2-F glass during melting or annealing temperature, glass-ceramic composite type material is obtained instead of getting superior glass phase (McDowell and Beall, 1969; Mcmillan, 1979; Aktas et al., 2019).

The general form of nucleation in glass-forming systems is achieved on the surface, however, volume nucleation is sometimes observed in the presence of heavy metal, which acts as a nucleating agent (McDowell and Beall, 1969; Mcmillan, 1979). However, certain glass compositions doped with nucleants exhibit volume nucleation without any heat treatment (Shelby, 2005; Beall, 2014). Chromium (Cr^{n+}), having variable oxidation states, can exhibit such nucleating behavior in a Si-O-Si-based system (Pingale et al., 1996). In a study on SiO_2-B_2O_3-based glass system, (Aktas et al., 2019) demonstrated that 0–1 wt% Cr_2O_3-containing glasses are completely amorphous but Cr_2O_3 contents >1 wt% makes those glasses crystalline, i.e., glass-ceramic. For volume nucleation in glasses, the selection of nucleant, the amount of nucleant, as well as the melting temperature should also be crucially selected (Dantas et al., 2011; Garai et al., 2015c; Garai and Karmakar, 2016b). However, the controlled crystallization in silicate-based glass matrix is attended by efficient internal nucleation, often enabled by a small amount of a nucleating agent. The efficiency of the technique lies in the development of finely grained randomly oriented crystalline phase, which generally comes without voids, micro-cracks, or porosity (Mcmillan, 1979). Glass-ceramics containing such fine-grained dense microstructures are highly desired for supporting marvelous thermal, mechanical, and electrical properties. In order to ascertain the fine-grained microstructures within devitrified glass phase, it is essential to ensure that nucleation of the crystal development occurs throughout the body of the glass (Garai et al., 2015c; Garai and Karmakar, 2016b). The attendance of nucleation catalysts in the glass, particularly of K_2O-MgO-B_2O_3-SiO_2-F system, greatly helps to control the crystallization process and allows a wider range of glass compositions to be converted into glass-ceramics (McDowell and Beall, 1969; Mcmillan, 1979).

The crucial criteria for the controlled crystallization process are high nucleation frequency, which should be uniform throughout the glass matrix; very uniform crystallite size; and very small crystallite dimensions, in particular, only a few micrometers or nanometers (Shelby, 2005; Garai and Karmakar, 2016b; Garai et al., 2015a). The primary process of controlled crystallization in K_2O-MgO-B_2O_3-SiO_2-F glass lies in controlling the microphase or nanophase separation. This is achieved by the specific selection of the base glass, specific additives as dopants, and a suitable temperature schedule. Regarding the exploration of microphase separation phenomenon in the K_2O-MgO-B_2O_3-SiO_2-F glasses, the composition of the microphases in the glass tends toward that of a more stable chemical compound (Dantas et al., 2011; Garai et al., 2015c).

Previous report is succeeded to establish the theory of redox equilibrium between the trivalent and hexavalent chromium (Cr^{+3}-Cr^{+6}) in silicate and borate glasses (Nath and Douglas, 1965; Wu et al., 1995; Murata et al., 1997; Rezvani et al., 2005; Hubert et al., 2014). The existence of tetravalent chromium has also been reported in aluminate-based glasses (Wu et al., 1995; Rezvani et al., 2005). In a crystallization study of SiO_2-Al_2O_3-CaO-MgO glasses, (Rezvani et al., 2005) established that Cr_2O_3 has significant effects on developing crystalline phases. Murata et al. (1997) investigated the effects of composition on the valence state of Cr-ions in multi-component oxide-based glasses (e.g., silicate, borate, phosphate, borosilicate, boro-aluminate,

aluminate, alumino-silicate, etc.). In a similar-type study, Hubert et al. (2014) pointed out that the divalent chromium content (Cr^{2+}) in SiO_2-Al_2O_3-Na_2O-CaO-MgO-Fe_2O_3-Na_2S glass melt has some effects on the melting at high temperature.

In present report, the gradual substitution of Al^{3+} ion by Cr^{6+} ionin K_2O-MgO-Al_2O_3-B_2O_3-SiO_2-Fsystem is studied. Due to the Cr^{6+} addition in such glasses, the relevant variation of the dilatometric thermal properties are explicated and correlated with differential scanning calorimetry (DSC). The self-crystallization propensity of such chromium-doped SiO_2-MgO-Al_2O_3-B_2O_3-K_2O-F glasses without heat-treatment is demonstrated by characterizing the techniques of X-ray diffraction (XRD), Fourier transform infrared spectroscopy (FTIR), and EDX experiments.

EXPERIMENTAL

The K_2O-MgO-Al_2O_3-B_2O_3-SiO_2-F glasses based on the composition shown in **Table 1** were synthesized by conventional melt-quench technique using highly pure reagent-grade fine chemicals. Most of the chemicals used were in the form of oxides, hydroxides, and carbonates as precursor material: SiO_2 (Quartz Powder, LobaChemie, Mumbai, India), $Al(OH)_3$ (97%, LobaChemie, Mumbai, India), $Mg(OH)_2$ (97%, LobaChemie, Mumbai, India), H_3BO_3 (99.5%, LobaChemie, Mumbai, India),K_2CO_3 (98%, LobaChemie, Mumbai, India), MgF_2(99.9%, LobaChemie, Mumbai, India), and $K_2Cr_2O_7$ (99%, E. Merck Ltd., Mumbai, India). The chemicals used were directly used for batch preparation without any further purification. All the glasses shown in **Table 1** were melted in a platinum (Pt) crucible (without lid) in an electrically heated raising hearth furnace at 1570°C for a 2-hour duration, followed by casting on a graphite mold in open-air atmosphere (at room temperature). The melts were further annealed at 600°C (2 h) for removing the internal stress generated during sudden quenching. The photograph of the synthesized glasses after annealing is exhibited in **Figure 1**, which clearly demonstrates the opaque nature of the monolith specimens in visible region.

Annealed glasses were characterized for various physical, thermal, and spectroscopic properties: density, DSC, dilatometry, FTIR, XRD, scanning electron microscopy (FESEM), energy dispersive X-ray analysis (EDS), and nano-indentation and micro-indentation study. Finely powdered (particle size, <60 μm) glass samples were subjected to DSC study (DSC, Setaram Labsys, Setaram Instrumentation, Caluire, France) in open air, from 30 to 1200°C at 10°C/min to obtain the phase transformation temperature. The glass transition feature (T_g), dilatometric softening point (T_d), and thermal expansion coefficient (CTE) values were evaluated using cylinder shaped bulk samples of length of ∼25 mm and diameter of ∼6 mm, using a horizontal dilatometer, NETZSCH DIL 402 PC (NETZSCH-Gerätebau GmbH, Germany) at a heating rate of 5°C/min (with an accuracy of ±1%).

X-ray diffraction analysis was recorded for the qualitative analyses of crystalline phases in studied glasses, using an XPERTPRO MPD diffractometer (PANalytical, Almelo, Netherlands) operating with Ni-filtered CuKα = 1.5406 Å radiation as the X-ray source at 40 kV and 40 mA current. Crystalline phases were analyzed in 2θ range of 5–90° (using a scan rate of 30 s-per-step) with a step size of 0.05° at a temperature of ∼25°C.

An FTIR transmission spectra of glass samples was recorded by FTIR spectrometer (Model 1615, Perkin-Elmer Corporation, Norwalk, CT, United States) at a resolution of ±2 cm^{-1} after 16 scans in the wave number range of 400 to 2000 cm^{-1}. The FTIR analysis was done using the transparent thin pellet (prepared by uniaxial hydraulic press, providing hand pressure of ∼10 tons) made by the mixture of glass powder and KBr in an approximate volume proportion of ∼1:300.

The morphology of the glasses was examined with an FESEM (FESEM model S430i, LEO, CEA, United States). Prior to the SEM investigations, the glass samples were polished and chemically etched by 2 vol.% aqueous HF solution for 10 min. To dictate the existing elements (K, Mg, Al, Si, O, F, and Cr) in the glass matrix, qualitative elemental composition analysis was performed using EDS analysis using the EDS detector attached with FESEM microscope. Density (*d*) of the investigated glass bulk samples was determined (with measurement error ± 0.7%) by the Archimedes principle using distilled water as immersion liquid.

Nano-indentation was performed from the polished (mechanical grinding and polishing) samples of base glass (Cr-0) plus Cr-containing glass-ceramics (Cr-2, Cr-4, and Cr-7) using a Berkovich indenter tip of radius 100 nm and angle 142.3° (Hystron, Model No. TIN 50 Triboindenter, United States). The indentation was carried out with an applied force of 5 mN and dwell time of 10 s, followed by constant unloading. In order to increase statistical significance of the data, indentations were obtained from various locations within the specimen surface. A total of 20 indentations were taken at any given location following a 4 × 5 square matrix pattern. Standard indentation *P*-h curves were generated from the load (*P*)-controlled nano-indentation tests, and the corresponding measurements of indentation depth (h). The hardness (*H*) and Young's moduli (*E*) were determined from the *P*-h curves based on the Oliver-Pharr method (Oliver and Pharr, 1992).

Vickers micro-hardness of glasses was estimated (with a measurement error of ±5%) using micro-indentation hardness testing system (UHL VMHT, Walter UHL). For each sample, 10 micro-indentions were taken along a straight line with constant 10-μm spacing under identical loading condition

TABLE 1 | Composition of studied alkaline borosilicate glasses, K_2O-MgO-Al_2O_3-B_2O_3-SiO_2-F with varying $K_2Cr_2O_7$ contents.

Sample No.	Composition (mol%)						
	MgO	B_2O_3	SiO_2	MgF_2	K_2O	Al_2O_3	$K_2Cr_2O_7$
Cr-0	20	10	44	12	7	7	–
Cr-2	20	10	44	12	5	5	2
Cr-4	20	10	44	12	3	3	4
Cr-7	20	10	44	12	0	0	7

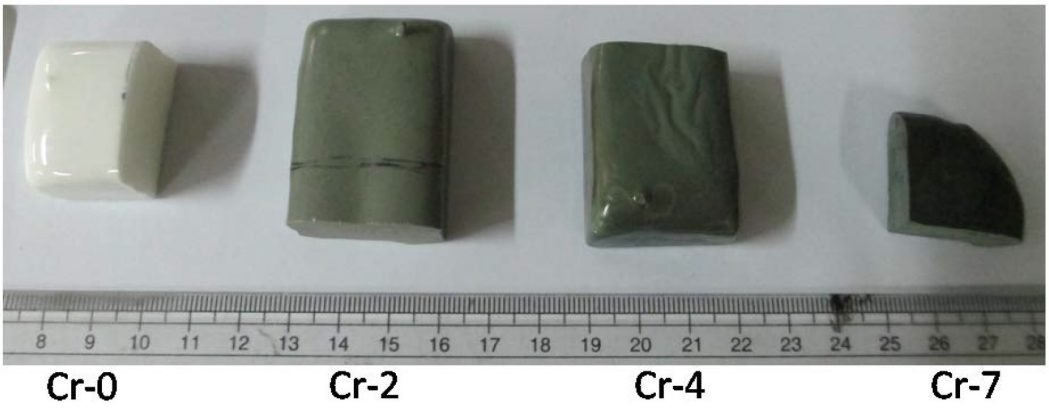

FIGURE 1 | Photograph of annealed K_2O-MgO-Al_2O_3-B_2O_3-SiO_2-F glass monoliths varying K_2O, Al_2O_3 and $K_2Cr_2O_7$ concentration; showing their opaque nature (for composition see **Table 1**).

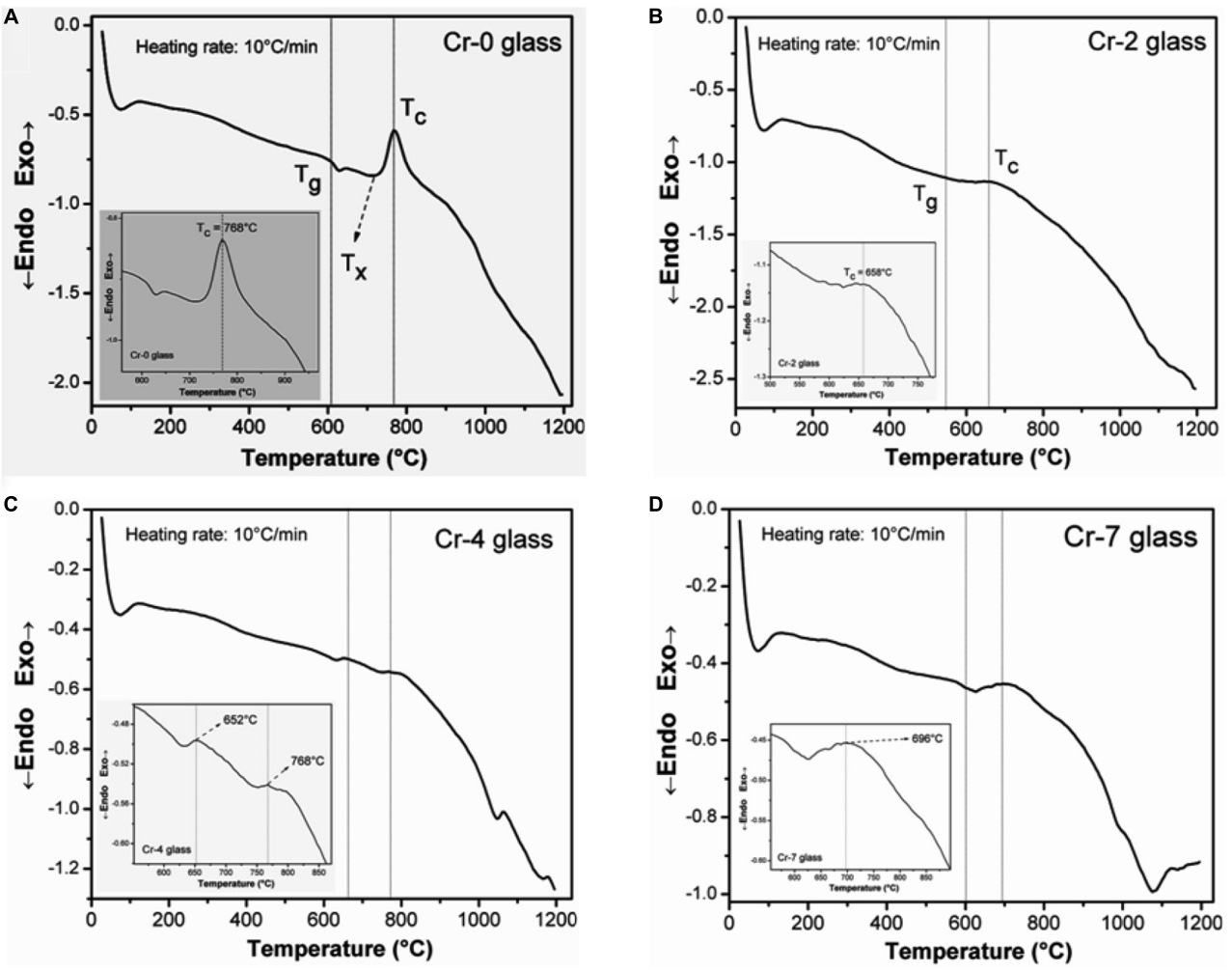

FIGURE 2 | Differential scanning calorimetric (DSC) thermogram of K_2O-MgO-Al_2O_3-B_2O_3-SiO_2-F glasses containing **(A)** 0 mol%, **(B)** 2 mol%, **(C)** 4 mol%, and **(D)** 7 mol% chromium content, showing the glass transition region (T_g), crystallization onset point (T_x) and crystallization exothermic temperature, T_c (for composition see **Table 1**).

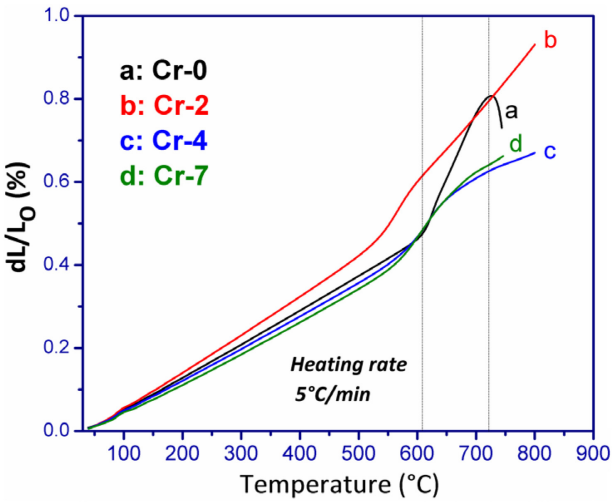

FIGURE 3 | Comparison of dilatometric thermal expansion trend (as a function of temperature) of K_2O-MgO-Al_2O_3-B_2O_3-SiO_2-F glasses with and without containing $K_2Cr_2O_7$ content; showing the disappearance of softening point temperature in attendance of chromium content (for composition see **Table 1**).

(= 500 g) in vertical direction under 10-second dwell time. The diagonals of different indents were carefully measured using the instrument attached optical microscope and consequently the micro-hardness values were calculated using the standard Eq. 1 for the Vickers geometry.

$$HV = \frac{1.854P}{d^2} \quad (1)$$

Where HV is the Vickers hardness number (VHN) in kg/mm^2. P is the normal load in g, d is the average diagonal length of the indentation in mm. Here, the HV value obtained/100.1 = Vickers hardness in GPa.

RESULTS AND DISCUSSION

To establish the variation in thermal properties owing to the Cr^{6+}- addition substituting Al^{3+} in SiO_2-MgO-Al_2O_3-B_2O_3-K_2O-F system, the annealed glass samples were experienced by non-isothermal DSC (using powder) and dilatometric (using bulk pellet) study. **Figures 2A–D** represent the DSC result of Cr-0, Cr-2, Cr-4, and Cr-7 glasses, respectively. The DSC pattern of Cr-0 glass (**Figure 2A**) is exceedingly different compared to other chromium-doped glasses. As seen from **Figure 2A**, the characteristic endothermic hump corresponding to glass transition is initiated at 585–590°C and ended at its minimum point 627°C. From the onset of this endothermic hump, the glass transition temperature (T_g) is estimated as 610 ± 2°C for Cr-0 glass. After the glass transition range (endothermic hump), an exothermic peak is initiated corresponding to crystallization (Murata et al., 1997; Pang et al., 2002). Onset of that crystallization (T_x) arch for Cr-0 glass is estimated as 716 ± 2°C with the highest point at 768 ± 2°C. Temperature difference between T_g and T_x corresponds to glass phase stability which is estimated 106 ± 2°C for Cr-0 glass (Shelby, 2005; Garai and Karmakar, 2016b). In case of Cr-doped system, the appearance of glass transition hump (DSC) is exceedingly different compared to Cr-0. The hump for Cr-2/Cr-4/Cr-7 in **Figures 2B–D** is insignificant to define those as amorphous material; however, the slight endothermic humps that appeared are an indication of residual glassy phase. As detailed in the experimental section, all as-quenched glasses were annealing heat-treated, and after annealing, the Cr-containing glasses were found crystallized. The crystallization in those glasses could have occurred both during cooling or annealing heat-treatment. Cr-0 glass, which is a typical boro-alumino-silicate system (K_2O-MgO-Al_2O_3-B_2O_3-SiO_2-F), is not crystallized upon such annealing temperature (Garai et al., 2015c; Garai and Karmakar, 2016b). Hence, Cr-0 is practically glass but Cr-2, Cr-4, or Cr-7 are not glass, rather those are glass-ceramic composite (Garai et al., 2018b; Aktas et al., 2019), and the endothermic and exothermic peaks in **Figures 2B–D** are due to minor residual glass phase. In a similar study on borosilicate system, (Aktas et al., 2019) argued that 0–1 wt% Cr_2O_3-containing borosilicate glasses are completely amorphous, but Cr_2O_3 contents of >1 wt% makes those glasses crystalline. In the present case, the crystallization for Cr-doped glasses could have occurred both during cooling or annealing heat-treatment. For Cr-0 glass, the exothermic maximum is estimated at 768 ± 2°C corresponding to crystallization temperature (Garai et al., 2018b). As is evident from DSC of Cr-2 to Cr-7 presented in **Figures 2B–D**, a slight exothermic range can be refereed at around 755–760°C for a Cr-2 system (**Figure 2B**), but that is not characteristic as an initiation of crystallization range. Lin et al. (2018) similarly studied DSC on Cr_2O_3-doped MgO-Al_2O_3-SiO_2-B_2O_3 glasses and argued that the incorporation of Cr-ion, as a modifier, can break the glass network and finally result in the decreased glass phase stability. In the present composition, Cr-4 contains 4 mol% $K_2Cr_2O_7$, and such optimum chromium contents were the reason for its more crystalline nature, as it appears in DSC thermograph (**Figure 2C**). Thus, 4 mol% $K_2Cr_2O_7$ is optimum for nucleation (under annealing temperature) in the present composition; further, Cr- addition does not confer for self-nucleation and crystallization support. The DSC appearance of Cr-7 system (**Figure 2D**) articulates this point.

TABLE 2 | Coefficient of thermal expansion (CTE) values of K_2O-MgO-Al_2O_3-B_2O_3-SiO_2-F glasses, with and without $K_2Cr_2O_7$ content.

Temp. Range	CTE value CTE (×10^{-6}/K)			
	Cr-0	Cr-2	Cr-4	Cr-7
50–200°C	7.66	8.51	7.26	7.28
50–300°C	7.79	8.72	7.40	7.31
50–400°C	7.91	8.89	7.54	7.56
50–500°C	8.01	9.11	7.66	7.77
50–600°C	8.17	10.69	8.28	8.41
50–700°C	11.56	11.49	8.77	10.62
50–800°C	–	12.24	9.18	10.53

TABLE 3 | XRD peaks and corresponding planes of different crystalline phases developed in $K_2Cr_2O_7$-containing K_2O-MgO-Al_2O_3-B_2O_3-SiO_2-F glasses.

Peak Position (2θ)	Corresponding planes	Crystalline phase	JCPDS file
18.34, 30.28, 34.58, 35.88, 52.87	(101), (200), (211), (202), (312)	Potassium chromium fluoride (K_3CrF_6)	27–1354
18.34, 30.28, 35.88, 37.00, 43.54, 57.54, 63.14	(111), (220), (311), (222), (400), (511), (531)	Magnesium chromium oxide ($MgCr_2O_4$)	82–1529
35.88, 40.18, 43.54, 52.87, 63.14	(101), (111), (210), (211), (310)	Magnesium fluoride (MgF_2)	72–2231
23.00, 25.62, 30.28, 32.52, 37.00, 40.18, 57.54	(200), (120), (001), (220), (130), (121), (041)	Mullite ($3Al_2O_3.2SiO_2$)	82–0037

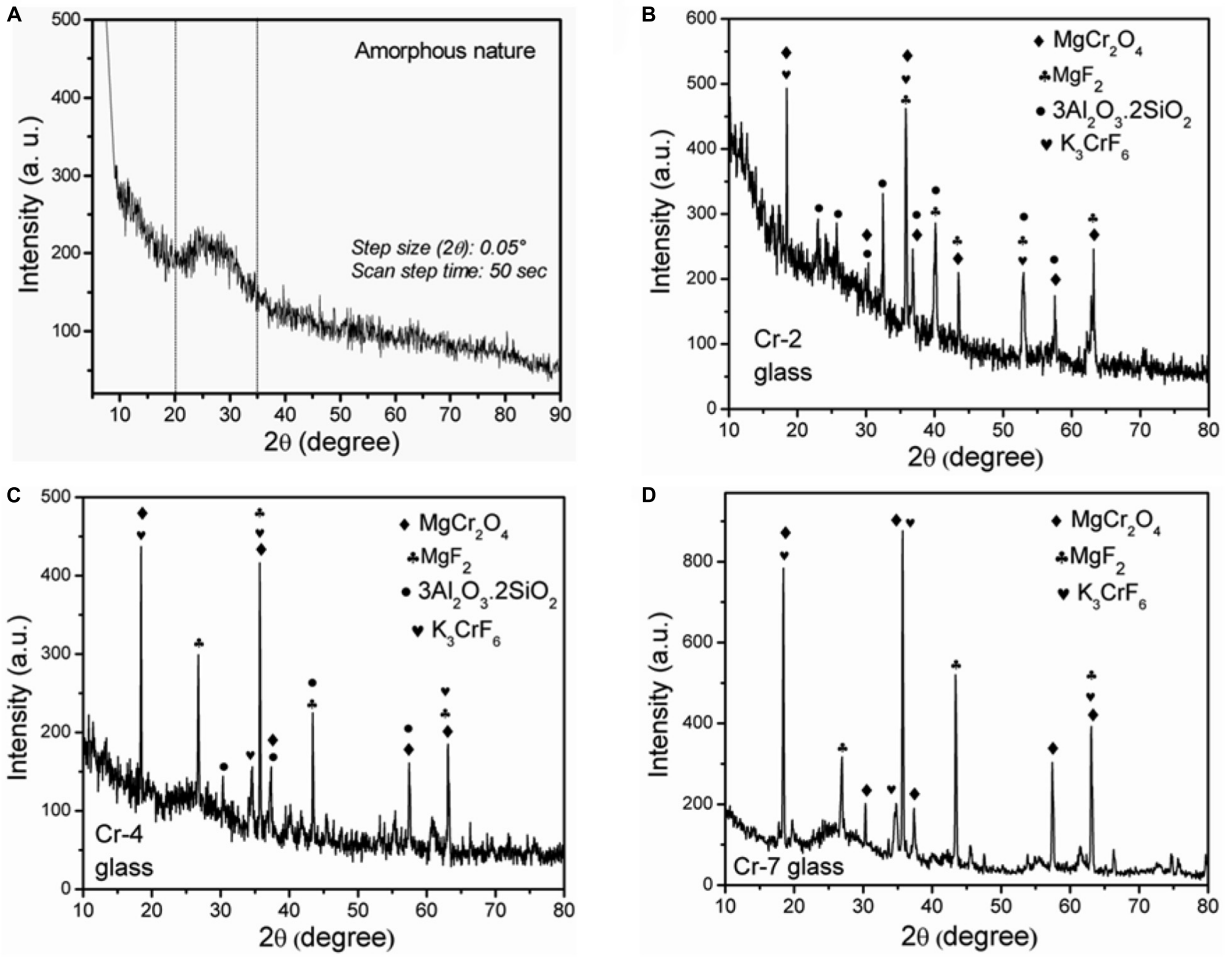

FIGURE 4 | XRD pattern of K_2O-MgO-Al_2O_3-B_2O_3-SiO_2-F glasses containing **(A)** 0 mol%, **(B)** 2 mol%, **(C)** 4 mol%, and **(D)** 7 mol% $K_2Cr_2O_7$ content, demonstrating the crystalline nature with the development of $MgCr_2O_4$, MgF_2, K3CrF_6, and mullite crystalline phases (for composition see **Table 1**).

The trend of thermal properties, particularly T_g, T_d, and CTE values of present glasses evaluated from dilatometric study is presented in **Figure 3**. From DSC results in **Figure 2**, glassy features are not observed for Cr-2/Cr-4/Cr-7 samples. So, characteristic glass transition and softening range have appeared dilatometric in a thermograph of Cr-0 glass only (**Figure 3a**), whereas the dilatometric curve for Cr-2, Cr-4, and Cr-7 glasses signify their glass-ceramic composite features (Lin et al., 2018; Aktas et al., 2019). The slight appearance of a glass transition hump for those in **Figure 3** signifies the residual glass phase only. Linear increase in CTE (up to 700°C) is obtained for all Cr- containing glasses; however, the linear trend is quite different for Cr-2 glass compared to others (**Table 2**). For Cr-0 glass, the CTE at 50–200°C is 7.66 × 10^{-6}/K and increased to 7.79, 7.91, 8.01, 8.17, and 11.56 × 10^{-6}/K at 50–300, 50–400, 50–500, 50–600, and 50–700°C, respectively. After T_d point (727 ± 1°C), it is decreased (**Figure 3a**). For Cr-2 where 2 mol% Al_2O_3 is substituted by $K_2Cr_2O_7$, the CTE is evaluated as 8.51 × 10^{-6}/K at 50–200°C. As the chromium addition caused self-nucleation, the CTE trend was similar to glass-ceramic (Garai and Karmakar, 2016b). At 50–300, 50–400, 50–500, 50–600, 50–700, and 50–800°C, the CTE value was evaluated as 8.72, 8.89, 9.11, 10.69, 11.49, and 12.24 × 10^{-6}/K for Cr-2 glass. When 4 mol% Al_2O_3 is substituted by $K_2Cr_2O_7$, more crystallinity is accomplished in

the glass. CTE of Cr-4 glass was thus evaluated as 7.26, 7.40, 7.54, 7.66, 8.28, and 8.77 and 9.18 × 10^{-6}/K at 50–200, 50–300, 50–400, 50–500, 50–600, 50–700, and 50–800°C, respectively. When total Al_2O_3 of SiO_2-MgO-Al_2O_3-B_2O_3-K_2O-F system is substituted by $K_2Cr_2O_7$, the CTE value is evaluated as 7.28, 7.31, 7.56, 7.77, 8.41, and 10.62, and 10.53 × 10^{-6}/K at 50–200, 50–300, 50–400, 50–500, 50–600, 50–700, and 50–800°C, respectively. Here, the interesting point to note that CTE of Cr-0 and Cr-2 glass is comparable in 50–700°C, whereas the same is low for Cr-4 glass and became high for Cr-7. This is because Cr-0 is glass and its softening range starts at around 670–680°C. So, the CTE is large at 50–700°C. But Cr-2 to Cr-7 is basically glass-ceramic or in true senses, the glass-ceramic composite (Garai et al., 2018b; Aktas et al., 2019). These contain different crystalline phases in the matrix body and thus, the CTE depends on crystalline phases as well as the residual glass phase. So, Cr-2 possesses CTE at 50–700°C is 11.49 × 10^{-6}/K. However, 4 mol% $K_2Cr_2O_7$ is optimum Cr-concentration in present composition for self-nucleation to attain inherent strength. So the structural relaxation with temperature is comparatively lower in Cr-4 system and possess CTE = 9.18 × 10^{-6}/K at 50–700°C.

Linear increase of CTE up to 700–900°C, the SOFC operation temperature, is one of the prime requisites for high temperature application like as SOFC. The large CTE (>11 × 10^{-6}/K) as observed in the Cr-2 system, is well-matched with SOFC components like electrodes (Ni/Fe), solid electrolytes (YSZ), interconnect (Crofer-22APU), etc., during operating temperature ∼700–900°C and thus this glass containing Cr- can suitably act as SOFC sealant. In brief, two major points are drawn from DSC and dilatometric observation: (i) Cr- addition ($K_2Cr_2O_7$) can cause self-nucleation in K_2O-MgO-B_2O_3-SiO_2-MgF_2-Al_2O_3 composition with 4 mol% as optimum Cr-concentration, and (ii) the 2 mol% $K_2Cr_2O_7$-containing K_2O-MgO-B_2O_3-SiO_2-MgF_2-Al_2O_3 system can act as suitable SOFC sealant.

The amorphous and crystalline nature of the present glasses was confirmed by an XRD study. As is evident from **Figure 4**, corresponding to Cr-0 glass, the broad hump appeared at (2θ) 20–35°C signifies the amorphous nature. Based on DSC and dilatometric experiments, it has already been pointed out that nucleation is required to initiate the crystallization that occurs in chromium containing glasses. And the crystallization could have occurred both during cooling or annealing heat-treatment (Lin et al., 2018; Aktas et al., 2019). Thus, crystalline nature is demonstrated by Cr-2, Cr-4, and Cr-7 glasses as depicted **Figures 4B–D**. Based on XRD observation, (Aktas et al., 2019) demonstrated that 0–1 wt% Cr_2O_3-containing borosilicate glasses are completely amorphous, but Cr_2O_3 contents of >1 wt% make those glasses crystalline, i.e., glass-ceramic. As is evident from **Figure 4B**, the characteristic peaks appeared at (2θ) 18.34, 30.28, 35.88, and 52.87°C are attributed to the crystalline planes (101), (200), (202), and (312) of crystalline phase potassium chromium fluoride, K_3CrF_6 (molecular weight of 283.28; JCPDS-PDF file number 27–1354, tetragonal body centered lattice; lattice parameter a = 6.047Å, c = 8.620Å). All the chromium-containing glasses were found to be multi-crystalline (**Table 3**). The crystalline peaks appeared (**Figure 5a**) at (2θ) 18.34, 30.28, 35.88, 37.00, 43.54, 57.54, and 63.14° are attributed to the crystalline planes (111), (220), (311), (222), (400), (511), and (531) of magnesium chromium oxide, $MgCr_2O_4$ (molecular weight = 192.29; JCPDS-PDF file number = 82–1529, face-centered cubic lattice; cell parameter a = 8.334 Å) (Pingale et al., 1996). During the annealing heat treatment, MgF_2 crystals are precipitated as primary crystalline phase (Mcmillan, 1979;

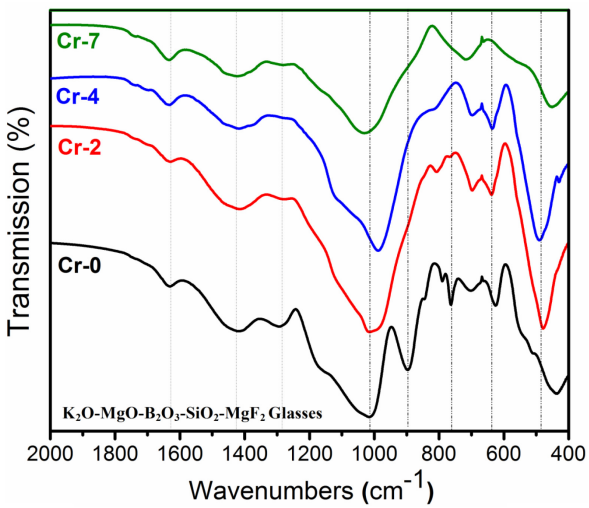

FIGURE 5 | FTIR pattern (in 400–2000 cm^{-1}) of K_2O-MgO-Al_2O_3-B_2O_3-SiO_2-F glasses with and without containing $K_2Cr_2O_7$ content; showing significant variation in the appearance of transmission band with $K_2Cr_2O_7$ concentration (for composition see **Table 1**).

TABLE 4 | Fourier transform infra-red transmission bands and respective assignments for K_2O-MgO-Al_2O_3-B_2O_3-SiO_2-F glasses with and without $K_2Cr_2O_7$ content.

Band position (cm^{-1})	Band assignment
450–500	Si-O-Si bending vibration modes of [SiO_4] unit (Fuxi et al., 1982; Xiu et al., 2006; Garai and Karmakar, 2016b).
620–650	Stretching vibration of Al-O bond of [AlO_4] unit (Tarte, 1967).
690–720	Stretching vibration of Si-O-B linkage (Xiu et al., 2006).
750–770	Al-O stretching vibration of [AlO_6] octahedral unit (Tarte, 1967).
790–820	Stretching vibration of the tetrahedral [BO_4] (Gautam et al., 2012).
890–920	Si-O asymmetric stretching mode of the NBOs. (Gautam et al., 2012).
980–1020	Si-O-Si asymmetric stretching of [SiO_4] unit (Tarte, 1967; Fuxi et al., 1982; Motke et al., 2002; Kumar et al., 2008; Laoot et al., 2011; Gautam et al., 2012; Garai and Karmakar, 2016b).
1280–1300	Anti-symmetric stretching of Si-O-Si of [SiO_4] (Tarte, 1967; Laoot et al., 2011; Gautam et al., 2012; Garai and Karmakar, 2016b)
1410–1430	B-O stretching of tri, tetra and pentaborate groups (Garai and Karmakar, 2016b).
1620–1640	H-O-H stretching vibration of molecular water (Laoot et al., 2011).

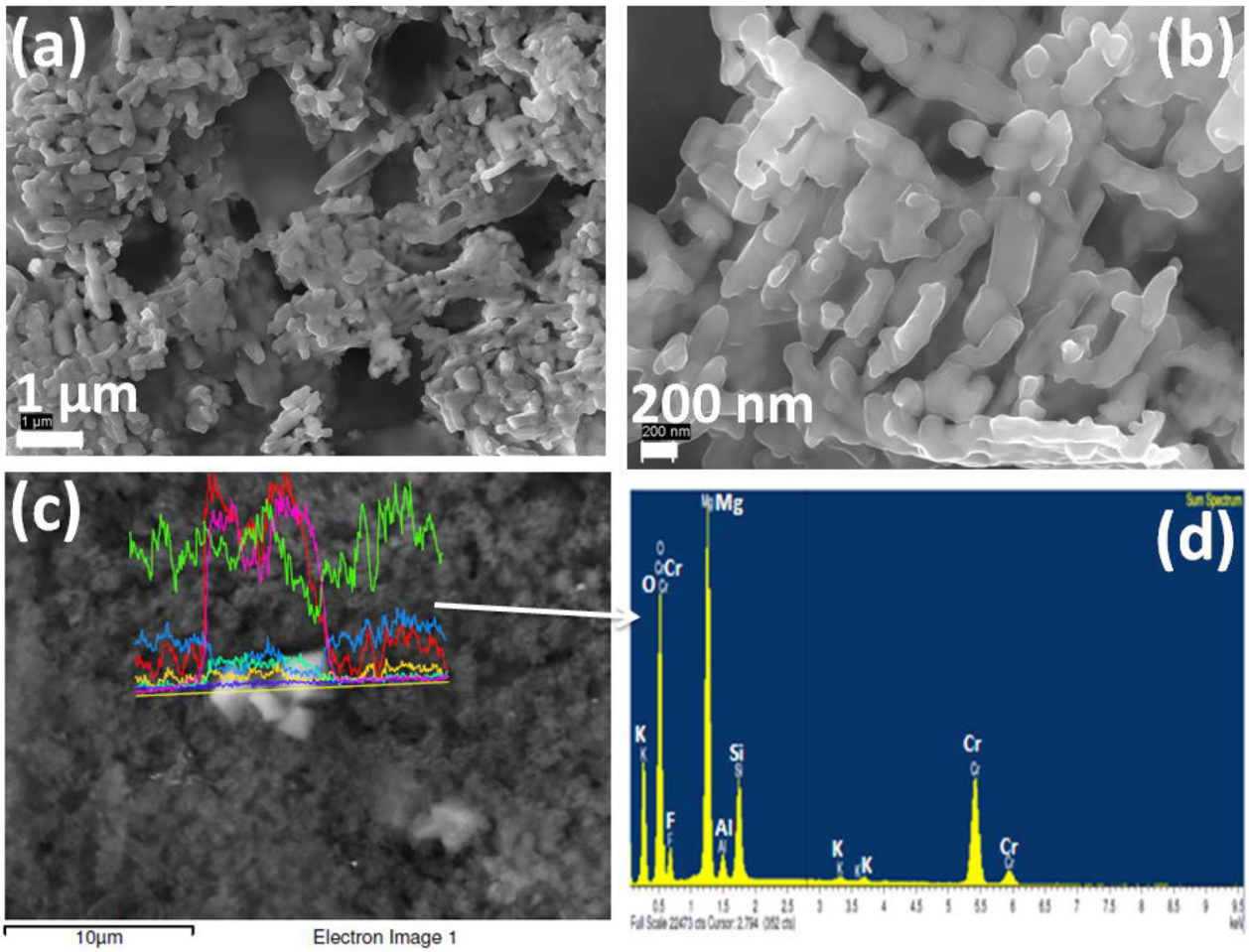

FIGURE 6 | (a,b) FESEM photomicrographs (in 1 μm and 200 nm) and **(c,d)** EDX pattern of K_2O-MgO-Al_2O_3-B_2O_3-SiO_2-F glass containing 2 mol% $K_2Cr_2O_7$ content, Cr-2; showing the dispersed crystalline phases ($MgCr_2O_4$, MgF_2, K_3CrF_6 and mullite).

Garai et al., 2015c; Garai and Karmakar, 2016b). As seen in **Figure 4**, the characteristic peaks appeared at (2θ) 35.88, 40.18, 43.54, 52.87 and 63.14° are ascribed to the phase reflection from (101), (111), (210), (211), and (310) planes of magnesium fluoride, MgF_2 (molecular weight = 63.30, tetragonal primitive system; JCPDS-PDF file number = 72–2231, lattice parameter a = 4.621Å, c = 3.050Å. Another Al- and Si-enriched crystalline phase is also developed in these glasses during annealing temperature (Garai et al., 2015c). As seen from **Figures 4B,C**, the crystalline peaks appeared at (2θ) 23.00, 25.62, 30.28, 32.52, 37.00, 40.18, and 57.54°correspond to the crystalline planes (200), (120), (001), (220), (130), (121), and (041) of mullite ($3Al_2O_3.2SiO_2$; molecular weight = 319.54; orthorhombic primitive system, JCPDS-PDF file number = 82–0037; lattice parameter a = 7.543Å, b = 7.691Å, c = 2.884Å). With higher Cr-content inK_2O-MgO-B_2O_3-SiO_2-MgF_2-Al_2O_3 glass, the chromium enriched crystalline phases tend to develop more. As seen from **Figure 4C** (i.e., Cr-4 glass), the crystalline peaks appeared at (2θ) 18.52, 30.28, 35.88, 37.19, 43.54, 57.54, and 63.13° are attributed to the development of magnesium chromium oxide, $MgCr_2O_4$. Whereas, the characteristic peak at 2θ = 34.58° is appeared in addition to 18.52, 35.88, and 63.13° due to the phase reflection from (211) plane of potassium chromium fluoride, K_3CrF_6. For Cr-2 glass, the crystalline peak appeared at (2θ) 35.88° was associated with highest intensity, but for Cr-4 glass the peaks positioned at (2θ) 18.52 and 35.88° was appeared with almost same intensity. The characteristic peak at (2θ) 18.52° is mainly attributed to the development of magnesium chromium oxide ($MgCr_2O_4$) and potassium chromium fluoride (K_3CrF_6). For the Cr-2 and Cr-7 system, mullite development decreased and K_3CrF_6/$MgCr_2O_4$ development increased, but mullite exists in Cr-4, whereas it is totally disappeared in Cr-7. So, the XRD pattern of Cr-7 glass presented in **Figure 4D** exhibits no appearance of mullite, phase because all the aluminum content is substituted by chromium. Thus, for Cr-7 glass, almost similar crystalline peaks appear for developing the chromium-enriched crystalline phases, i.e., $MgCr_2O_4$ and K_3CrF_6. The increase in the intensity of crystalline peaks at (2θ) 18.34, 35.70, and 63.14°clearly demonstrate the enhanced crystallization in presence of more

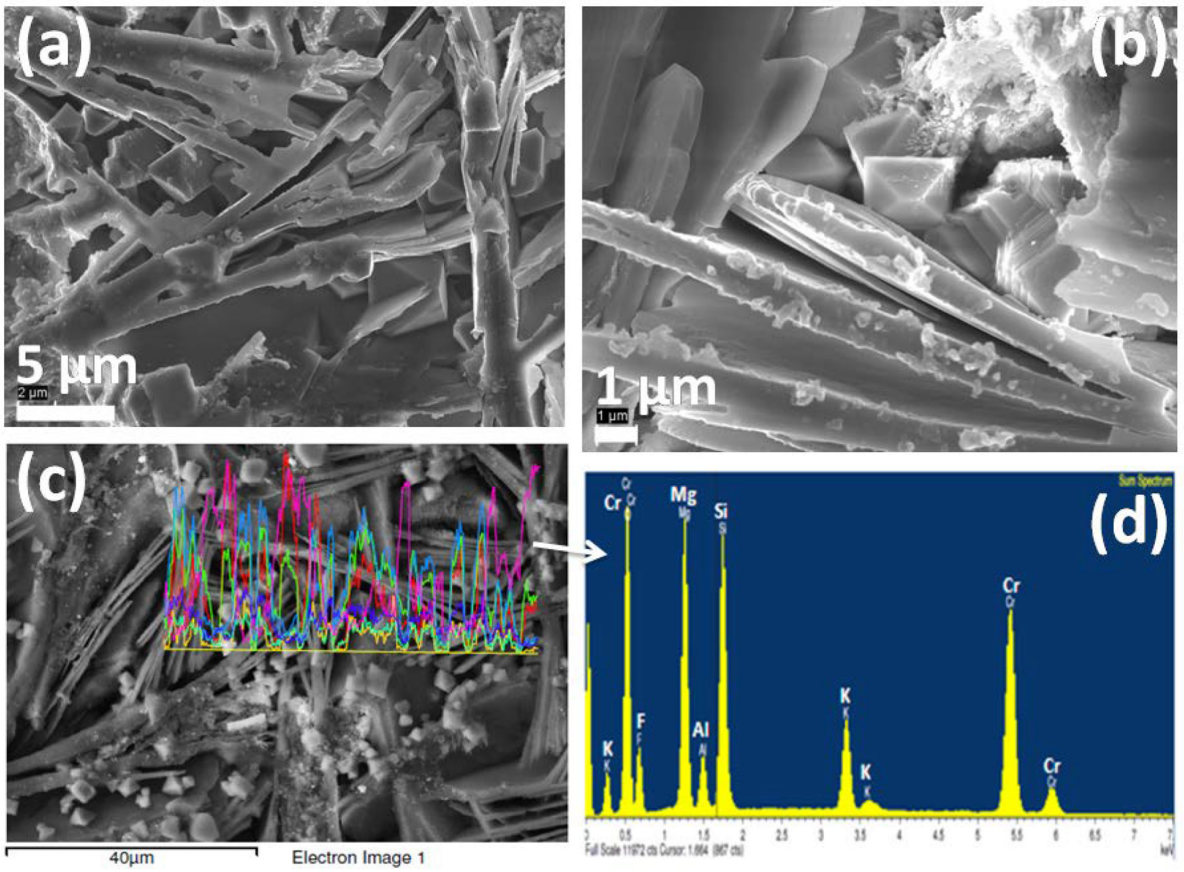

FIGURE 7 | (a,b) FESEM photomicrographs (in 5 and 1 μm) and **(c,d)** EDX pattern of K_2O-MgO-Al_2O_3-B_2O_3-SiO_2-F glass containing 4 mol% $K_2Cr_2O_7$ content, Cr-4; showing the dispersed crystalline phases ($MgCr_2O_4$, MgF_2, K_3CrF_6 and mullite).

chromium content, i.e., in Cr-4 and Cr-7 glasses compared to Cr-2 glass.

The room-temperature FTIR transmittance spectra in the wave-number range from 400 to 2,000 cm^{-1} for all the glasses were examined for structural elucidation. **Figure 5** shows that the FTIR pattern is almost similar for all the glasses after 1,000 cm^{-1}; however, the appearance of the bands is considerably different in the wave number range of 400 to 1,000 cm^{-1}. FTIR bands appeared for the glasses, and respective assignments are summarized in **Table 4**. The sharp transmission band at ∼450–500cm^{-1} for all the glasses corresponds to Si-O-Si bending vibrational modes of [SiO_4] tetrahedral (Fuxi et al., 1982; Xiu et al., 2006; Garai and Karmakar, 2016a). In the FTIR pattern of Cr-2 to Cr-7 glasses, a characteristic band appears at 620–650 cm^{-1}, and this is attributed to Al-O stretching vibration of [AlO_4] unit (Tarte, 1967). This band is present only in the case of glasses that contain Al-, which gives indirect evidence for the development of Si-O-Al inter-tetrahedral linkage (Shelby, 2005). This particular band at 620–650 cm^{-1} of Cr-0 is sharper than that of the Cr-2 and Cr-4 glasses because of higher Al_2O_3 content (7 mol%) in Cr-0 glass. In Cr-7, this band totally disappears because of missing Al- content, and hence, there is no Si-O-Al linkage (Garai et al., 2015c; Aktas et al., 2019). Si-O-Al and Si-O-B both are generally formed because of the boro-alumino-silicate system, as in the present case. Evidence for the formation of borosiloxane bonds (Si-O-B) is confirmed by the transmission bands positioned at 690–720 cm^{-1} (Xiu et al., 2006). To further stabilize on heating, 4-coordinated Al- atoms have a common tendency to be fitted into a 6-coordinated array. When [AlO_4] units tend to be converted into [AlO_6], they enter into the glass matrix controlled by Si-O-Si network. But, cannot be accommodated into the crystalline matrix in presence of chromium ion (Cr^{n+}) having large ionic radius (Shelby, 2005; Aktas et al., 2019). Aktas et al. (2019) studied FTIR on borosilicate glasses and established that 0–1 wt% Cr_2O_3 containing borosilicate glasses are completely amorphous (Si-O-Si), whereas Cr_2O_3 contents of >1 wt% make those glasses crystalline, i.e., glass-ceramic. As seen in **Table 4**, the characteristic band at ∼750–770 cm^{-1} appears in Cr-0 and gradually disappears in chromium containing glasses, i.e., Cr-2, Cr-4, and Cr-7. This particular band is assigned to Al-O stretching vibration of the tetrahedral [AlO_4] units (Tarte, 1967). Non-bridging oxygen (NBO) in the form of [BO_4] vibrations was observed at 790–820 cm^{-1}, and the absorption around 900 cm^{-1} indicates the formation of diborate groups in the glassy matrix (Gautam et al., 2012). The band positioned

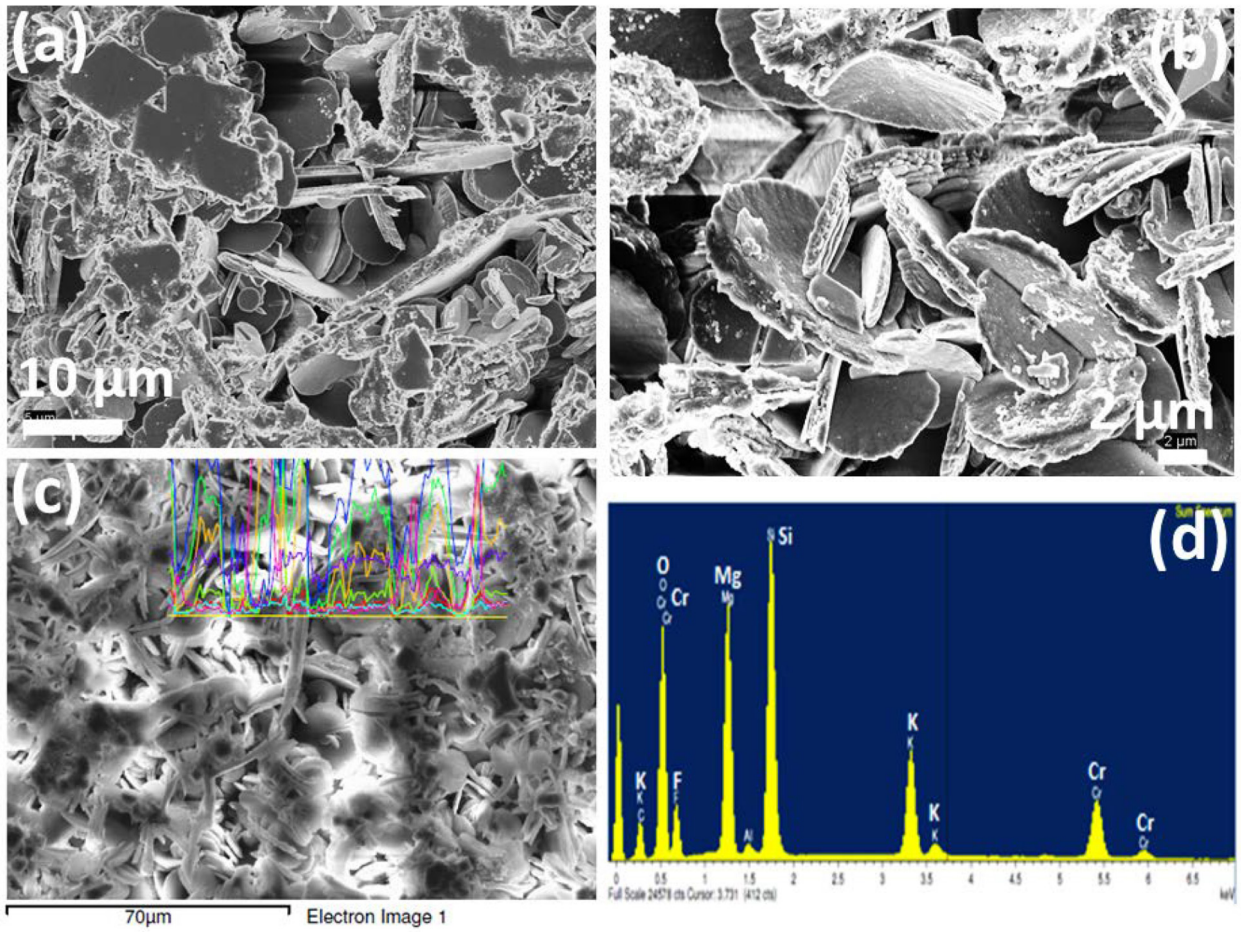

FIGURE 8 | (a,b) FESEM photomicrographs (in 10 and 2 µm) and **(c,d)** EDX pattern of K_2O-MgO-Al_2O_3-B_2O_3-SiO_2-F glass containing 7mol% $K_2Cr_2O_7$ content, Cr-7; showing the dispersed crystalline phases ($MgCr_2O_4$, MgF_2 and K_3CrF_6).

at 890–920 cm^{-1} furthermore indicates the Si-O asymmetric stretching mode of the NBOs (Kumar et al., 2008; Laoot et al., 2011; Gautam et al., 2012). FTIR spectra of all glasses exhibit a characteristic band centered at ∼988–1030 cm^{-1}, which is assigned to Si-O-Si asymmetric stretching vibration of [SiO_4] unit for amorphous silica (Tarte, 1967; Kumar et al., 2008; Laoot et al., 2011; Gautam et al., 2012). As seen from **Figure 5**, this characteristic band is exceedingly sharp, and this additional broadening is attributed to the stretching vibration of B-O linkage of tetrahedral [BO_4] unit having characteristic band at this region of ∼1,000–1,050 cm^{-1} (Fuxi et al., 1982; Motke et al., 2002). The band at about 1,000 cm^{-1} furthermore sharpens due to a stretching vibration of B-O-Si linkage in the glass system K_2O-MgO-Al_2O_3-B_2O_3-SiO_2-F (Gautam et al., 2012). Although chromium concentration is different in all the K_2O-MgO-B_2O_3-SiO_2-MgF_2-Al_2O_3 systems, the glass phase is predominately controlled by Si-O-Si phase, because the major composition of the sample is silicon oxide (**Table 1**). With IR spectra on Cr_2O_3-doped MgO-Al_2O_3-SiO_2-B_2O_3 glasses, Lin et al. (2018) demonstrated that the incorporated Cr^{3+} ions, as network modifiers, are located in the interstitial sites and have little impact on the network structure of such boro-alumino-silicate glasses. The broad transmission band is centered at 1,280–1,300 cm^{-1}, particularly for Cr-0 glass, and is ascribed to Si-O-Si anti-symmetric stretching vibration of [SiO_4] unit (Tarte, 1967; Laoot et al., 2011; Gautam et al., 2012; Garai and Karmakar, 2016a). The low-intensity band centered at 1,410–1,430 cm^{-1} can be attributed to B-O symmetric stretching vibration of tetrahedral [BO_4] units (Gautam et al., 2012; Garai and Karmakar, 2016a). The characteristic transmission band centered at ∼1620–1640 cm^{-1} in all the glasses is assigned to the H-O-H bending vibrational mode of water molecule (Laoot et al., 2011).

The above discussion strongly suggests that the SiO_2-MgO-Al_2O_3-B_2O_3-K_2O-F glass without Cr- content possess Si-O-Si and B-O-B networks, both of which maintain amorphous character. However, the predominant structure is formulated by Si-O-Si phase. When Al^{3+} is substituted with Cr^{6+} content, the Si-O-Al inter tetrahedral link formation is reduced, but major phase is controlled by Si-O-Si network. The self-nucleation and crystallization are accompanied more in the presence of a higher chromium concentration; and hence,

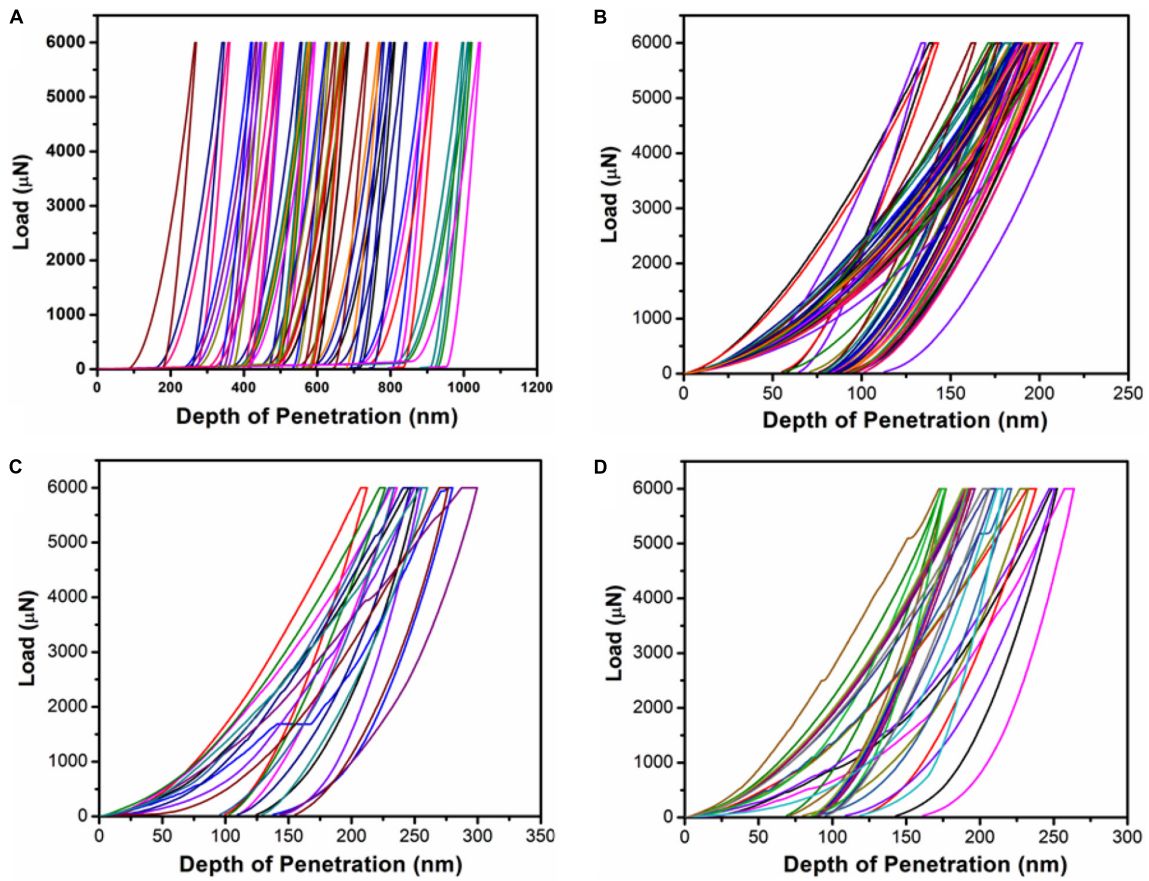

FIGURE 9 | P-h curves from nano-indentation tests using Berkovich indenter tip from K_2O-MgO-Al_2O_3-B_2O_3-SiO_2-F glasses with and without $K_2Cr_2O_7$; **(a)** Cr-0, **(b)** Cr-2, **(c)** Cr-4, and **(d)** Cr-7.

the 4-coordinated [SiO_4] and [AlO_4] bands are considerably tailored. Thus, Cr-0 to Cr-4 glasses exhibited sharp bands for Si-O and Al-O bond vibrations for the development of [SiO_4] and [AlO_4] units. Lin et al. (2018) studied DSC, XRD and IR observation on MgO-Al_2O_3-SiO_2-B_2O_3 glasses and established that 0–1 mol% Cr_2O_3-doped glass samples are predominated by amorphous network containing major functional groups [SiO_4] and [AlO4]. Based on a similar FTIR study, (Aktas et al., 2019) found that borosilicate glasses containing Cr_2O_3 contents <1 wt% are amorphous but become crystalline when containing Cr_2O_3 of >1 wt%. In the present composition, there is a large difference in the FTIR band appearance at 600–800 cm^{-1} for Cr-2 to Cr-7 glasses, being thus evidence for the effect of amorphous-to-crystalline phase transformation (Mcmillan, 1979; Aktas et al., 2019).

Since the phenomena of self-crystallization occurred under annealing heat treatment for studied glasses was caused by chromium ion, it is of interest to compare how their microstructures (FESEM) are changed with increased Cr-content. The cooling of these Cr-containing SiO_2-MgO-Al_2O_3-B_2O_3-K_2O-F melts tend to induce the spontaneous liquid–liquid phase separation, giving rise to heterogeneous phase formation initially with F-rich droplets (Garai et al., 2015a; Garai and Karmakar, 2016a). The crystalline planes (101), (111), (210), (211), and (310) identified in XRD pattern were due to MgF_2 phase. FESEM morphology of Cr-2, Cr-4, and Cr-7 glasses is presented in **Figures 6–8** respectively. As seen from **Figure 6a**, fine crystallite particles are dispersed randomly throughout the matrix in a "localized colony"-like arrangement. Over a higher magnification into **Figure 6a**, it is seen that rock-like 200–500 nm sized crystalline particles are parallel arranged (**Figure 6b**). Such interlocked types of morphology (with large CTE) makes this K_2O-MgO-B_2O_3-SiO_2-MgF_2-Al_2O_3 composition (Cr-2) useable as high temperature

TABLE 5 | Depth of penetration (h), Young's modulus and hardness measured from the nano-indentation tests on K_2O-MgO-Al_2O_3-B_2O_3-SiO_2-F glasses with and without $K_2Cr_2O_7$.

Sample	Contact Depth (nm)	Modulus (GPa)	Hardness (GPa)
Cr-0	619 ± 195	25 ± 10	0.6 ± 0.5
Cr-2	139 ± 16	94 ± 21	8.4 ± 2.3
Cr-4	170 ± 46	88 ± 22	6.3 ± 2.2
Cr-7	242 ± 65	58 ± 10	3.3 ± 1.5

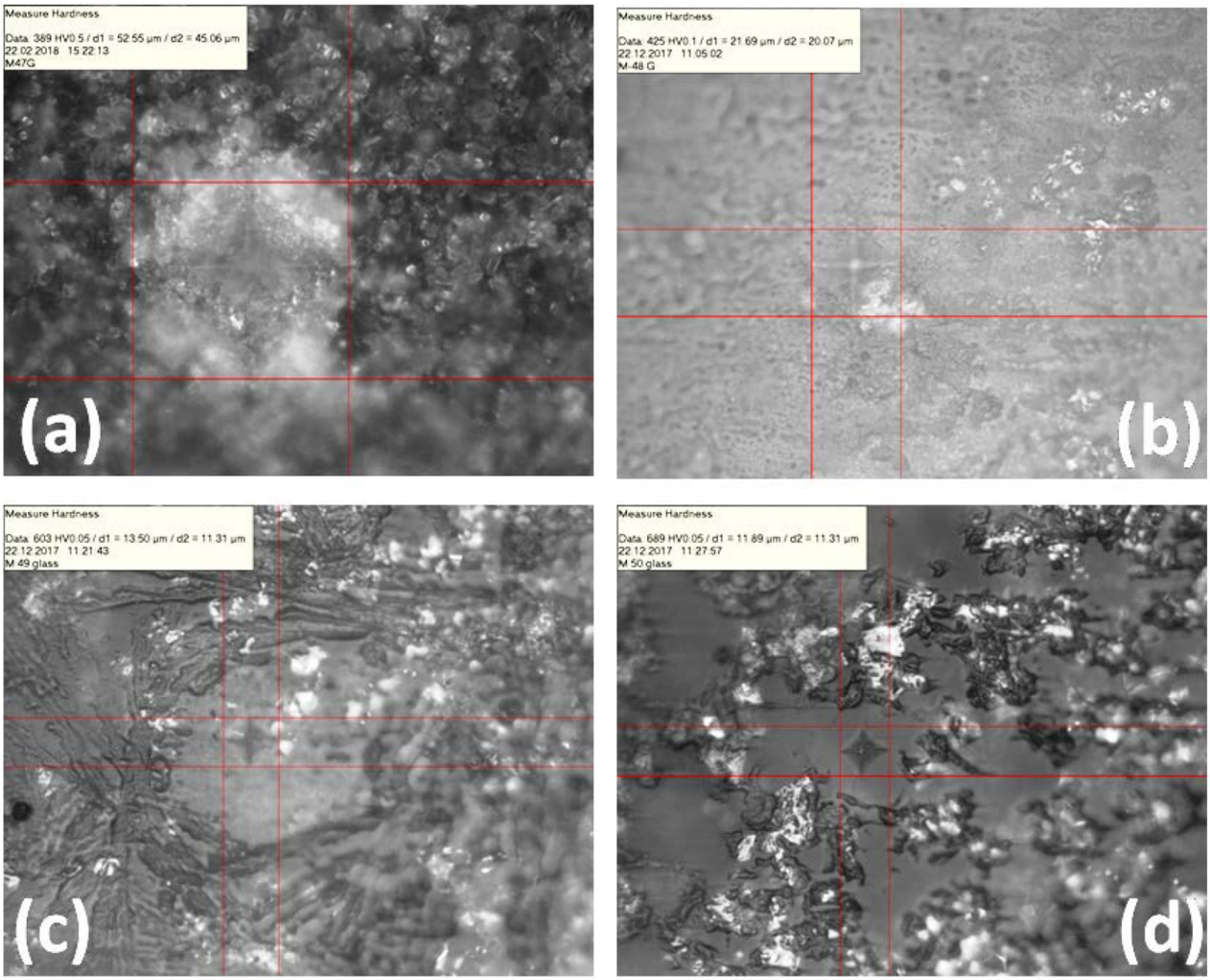

FIGURE 10 | Photograph of micro-hardness indentation impression on K_2O-MgO-Al_2O_3-B_2O_3-SiO_2-F glasses **(A)** Cr-0, **(B)** Cr-2, **(C)** Cr-4, and **(D)** Cr-7, showing the increasing crystallinity with chromium content (for composition see **Table 1**).

sealant (SOFC) (Kumar et al., 2008; Garai et al., 2015c; Garai and Karmakar, 2016b). From the EDS pattern presented in **Figure 6d**, the elements present in Cr-2 matrix are made out. Density of Cr-2 glass is estimated as 2.61 ± 0.02 $g.cm^{-3}$. Density of chromium (atomic radius = 1.28 Å) atom is 7.19 $g.cm^{-3}$, which is one of the reason for higher density of glass matrix with increase of Cr^{6+}content. Lin et al. (2018) explained a monotonic increase in bulk density (i.e., denser microstructure) of MgO-Al_2O_3-SiO_2-B_2O_3 glasses with increased Cr_2O_3 concentrations based on higher molar mass and lower molar volume. When 4 mol% Al_2O_3 is substituted with $K_2Cr_2O_7$, more chromium-containing crystalline phases were accessible to develop (Pingale et al., 1996; Rezvani et al., 2005). **Figures 7a,b** demonstrate the crystalline morphology of the Cr-4 system, which is composed of 5–10 µm-sized plate-like crystallites homogeneously arranged to provide a compact microstructure. Small amounts of plate-like crystals tend to combine by parallel arrangement to form a layered plate structure. The space between two layers can be predicted to be 500 nm to 1 µm. **Figure 7c** shows another type of 1 to 5 µm-sized crystals (rock-like) present in a lower quantity compared to plate-like crystals. The rock-like crystals of smaller dimension are dispersed in the vacant space created in between two or three layered-plate structures. The higher density of Cr-4 glass (= 2.63 ± 0.02 $g.cm^{-3}$) is, hence, attributed to such compact microstructural morphology (Karamanov et al., 1999; Garai et al., 2015a; Garai and Karmakar, 2016b). From the EDS pattern in **Figure 7d**, the elemental composition of crystalline phases developed in Cr-4 is confirmed. In the crystallization study of SiO_2-Al_2O_3-CaO-MgO glasses, Rezvani et al. (2005) established that Cr_2O_3 has significant effects on developing crystalline phases. In the Cr-7 system, total Al_2O_3 is substituted by $K_2Cr_2O_7$, and hence, $MgCr_2O_4$ and K_3CrF_6 phases are majorly developed (Karamanov et al., 1999). The interesting point noticed for Cr-7 glass is that the intensity of the XRD peak at (2θ) 43.54° is largely increased

(**Figure 4D**). As seen from **Figures 8a,b**, large number of mushroom-like crystals is distributed in an archetypal manner to furnish a highly compact microstructure. Karamanov et al. (1999) argued that Cr_2O_3 affects, as a strong nucleating agent in iron containing SiO_2-Al_2O_3-CaO-MgO-ZnO-PbO-Na_2O-K_2O, glass-ceramics. **Figure 8c** demonstrates the large variation in crystallite size (10–15 μm), as well as their orientation, where smaller-sized plates are mostly placed on the bigger ones. Such homogeneous arrangement of plate-shaped crystals can be attributed for highest-density value (= 2.66 ± 0.02 $g.cm^{-3}$) (Garai et al., 2015c). Comparing the EDS pattern of Cr-4 and Cr-7 glasses, the question may be raised of why the Cr- peak is higher in Cr-4 than that in Cr-7. This is due to typical crystalline morphology in the Cr-4 matrix. Size of some crystallite particles here are around 10–20 μm, and the quantity of such crystallites is sufficient to control the morphology. As evidenced from **Figure 7d**, the EDS pattern was directly taken from such crystallites–X ray beam (EDS) interaction so that Cr peak became high. But in case of Cr-7 sample, X-ray beams (EDS) probably trickled with smaller sized crystallites as well as amorphous (Si-O-Si) matrix. The large Si- peak (Si-O-Si) in **Figure 8d** justifies this.

The loading and unloading *P*-h curves from the nano-indentation tests on the SiO_2-MgO-Al_2O_3-B_2O_3-K_2O-F glasses are presented in **Figure 9**. As evidenced from the XRD and SEM observations, the base glass (Cr-0) is essentially an amorphous system, which, upon addition of Cr, converts to glass-ceramics. **Figure 9a** thus represents a loading-unloading *P*-h curve characteristic of Cr-0 glass with a much higher depth of penetration for the constant load of 5 mN. The low depth of penetration for Cr-2, Cr-4, and Cr-7 glass-ceramics on the other hand, suggests higher strength (**Figures 9b–d**), due to correspondingly higher crystallinity and compactness of the microstructures. For Cr-0 system (glass), the depth of penetration reached to ∼950 nm whereas for Cr-2, Cr-4, and Cr-7 glass-ceramics it is ∼200–250 nm (**Table 5**). Interestingly, both Young's modulus and hardness first increased when chromium (Cr-2) was added to the base glass (Cr-0) but decreases monotonically upon addition of further chromium (Cr-4 and Cr-7). This fact is ascribed to the change in morphology of the crystal phases.

Micro-hardness of glass/glass-ceramic materials is strongly dependent on strength, crystallinity and volume fraction of microstructure (Garai et al., 2015a, 2018a; Sasmal et al., 2016). Micro-hardness indentation impression for the studied glasses is presented in **Figures 10A–D**. For Cr-0 glass the micro-hardness is estimated 3.63 (±0.18) GPa; and for Cr-containing systems, it is obviously higher as those are crystalline in nature. Cr-2 matrix (**Figure 10B**) is composed of 200 to 500 nm-sized crystals dispersed randomly, and such arrangements are the reason for its lower micro-hardness value of 3.94 (±0.20) GPa (Garai et al., 2015a, 2018a). Cr-4 system is composed of 5 to 10 μm-sized plate-like crystals, arranged parallel to provide a compact microstructure, which caused its higher micro-hardness of 6.08 (±0.30) GPa (Garai et al., 2015a,b). In case of Cr-7 system, crystallites (sized 10–15 μm) are distributed in an archetypal manner where smaller sized plates are mostly placed on the bigger ones; such morphology is responsible for the micro-hardness value of 5.84 (±0.29) GPa (Garai et al., 2014, Garai et al., 2015a, 2015b). Thus, the microstructural variation governed the mechanical properties—in particular, contact depth, modulus, and hardness value. On addition of Cr-content, self-nucleation caused the considerable variation in microstructure and, hence, the mechanical properties (Karamanov et al., 1999; Garai et al., 2015c). The typical microstructure-driven mechanical properties (micro-hardness, 3.94 ± 0.20 GPa) make the Cr-2/Cr-4 glasses compatible for powder compact in a high-temperature sealing application like SOFC (Garai et al., 2014, 2015a; Sasmal et al., 2016).

CONCLUSION

The present work demonstrates the effect of addition of chromium (Cr) on the nucleation behavior; the alteration of microstructure; and the physical, thermal, and mechanical properties of SiO_2-MgO-Al_2O_3-B_2O_3-K_2O-F base glasses, where the gradual substitution of Al^{3+} ion is attempted via Cr^{6+} ion (in form of $K_2Cr_2O_7$), based on the similar ionic radius. The major conclusions are summarized below:

- In the presence of Cr^{n+}, self-nucleation was made possible in base glasses and the crystallization could have occurred both during cooling and annealing heat treatment (600°C). Glassy features were observed in dilatometric thermal properties (T_g, T_d, thermal expansion) without Cr-containing glass, whereas glass-ceramic like features were present for Cr-containing glasses. A similar observation is ascertained in DSC results.
- An XRD study confirmed that the base glass is amorphous, whereas Cr-doped glasses are crystalline. The main crystalline phases in such Cr-containing glasses were identified as $MgCr_2O_4$ and K_3CrF_6, along with MgF_2 and mullite ($3Al_2O_3.2SiO_2$).
- A dense microstructure containing 200 to 500 nm-crystals was obtained in 2 mol% $K_2Cr_2O_7$-containing glass. In higher Cr-containing glasses, the microstructure was more compact with 10 to 50 μm-plate like crystals. Crystallinity is increased with Cr-content, and thus, density also increased.
- Micro-hardness of the base glass (3.63 ± 0.18GPa) increased to 3.94–6.08 GPa in Cr- containing glasses.
- From nano-indentation measurements, hardness and Young's modulus were estimated to be 0.6 (±0.5) and 25 (±10) GPa, respectively, for base glass, which increased to the range of 3.3–8.4 and 58–94 GPa, respectively, for Cr-containing glasses.
- 2 mol% $K_2Cr_2O_7$-doped SiO_2-MgO-Al_2O_3-B_2O_3-K_2O-F glass showed large CTE (11.49–12.24 × 10^{-6}/K) and typical microstructure driven physical (density 2.61 ± 0.02 $g.cm^{-3}$) and mechanical properties (micro-hardness, 3.94 ± 0.20 GPa; Young's modulus, 94 ± 21 GPa) that make it suitable for high-temperature sealing application like that required in SOFC.

In brief, two major conclusions are drawn from this report: (i) Cr- addition ($K_2Cr_2O_7$) can cause self-nucleation in K_2O-MgO-B_2O_3-SiO_2-MgF_2-Al_2O_3 composition with 4 mol% as optimum Cr-concentration, and (ii) 2 mol% $K_2Cr_2O_7$ containing K_2O-MgO-B_2O_3-SiO_2-MgF_2-Al_2O_3 composition can act as suitable SOFC sealant.

DATA AVAILABILITY STATEMENT

The datasets generated for this study are available on request to the corresponding author.

AUTHOR CONTRIBUTIONS

BK planned the work. MG performed all the experimental work and relevant analysis of the results supervised by BK (for thermal and structural characterization), and involved in analyzing the mechanical characterizations supervised by SR. SR designed the experimental work for the mechanical properties. MG and SR involved in the manuscript preparation.

FUNDING

MG thankfully acknowledges DST-SERB for providing financial support under N-PDF Scheme (File Number: PDF/2016/003799).

ACKNOWLEDGMENTS

The authors thank Dr. K. Muraleedharan, Director, Dr. R. Sen, Head, Glass Division and Dr. R. N. Basu, Head, Fuel Cell and Battery Division of CSIR-CGCRI, Kolkata for their support to carry out this work. The authors like to acknowledge Central Research Facility (CRF) of Indian Institute of Technology (IIT) Kharagpur for providing the required mechanical characterization facilities.

REFERENCES

Aktas, B., Yalcin, S., Dogru, K., Uzunoglu, Z., and Yilmaz, D. (2019). Structural and radiation shielding properties of chromium oxide doped borosilicate glass. *Radiation Phys. Chem.* 156, 144–149.

Beall, G. H. (2014). Milestones in glass-ceramics: a personal perspective. *Int. J. Appl. Glass Sci.* 5, 93–103.

Dantas, N. O., Ayta, W. E. F., Silva, A. C. A., Cano, N. F., Silva, S. W., and Morais, P. C. (2011). Effect of Fe_2O_3 Concentration on the Structure of the SiO_2-Na_2O-Al_2O_3-B_2O_3 Glass System. *Spectrochim. Acta A Mol. Biomol. Spectrosc.* 81, 140–143. doi: 10.1016/j.saa.2011.05.074

Deubener, J., and Höland, W. (2017). Nucleation and crystallization of glasses and glass-ceramics. *Front. Mater.* 4:14. doi: 10.3389/fmats.2017.00014

Fuxi, G., Guosong, H., and Shizheng, C. (1982). Vibrational Spectra of Multicomponent Inorganic Glasses. *J. Non Cryst. Solids* 52, 203–210.

Garai, M., Ch Murthy, T. S. R., and Karmakar, B. (2018a). Microstructural characterization and wear properties of silver and gold nanoparticle doped K-Mg-Al-Si-OF glass-ceramics. *Ceramics Int.* 44, 22308–22317.

Garai, M., and Karmakar, B. (2016a). Development of fluorophlogopite mica nanocrystals in Zn-containing B_2O_3-Al_2O_3-SiO_2-K_2O-MgO-F glasses. *Nanospectrum* 1:97.

Garai, M., and Karmakar, B. (2016b). Rare earth ion controlled crystallization of mica glass-ceramics. *J. Alloys Comp.* 678, 360–369.

Garai, M., Maurya, A. K., and Roy, S. (2018b). Zn 2+-controlled crystallization and microstructure in K-Li-Mg-B-Si-Al-F glass. *MRS Adv.* 3, 3525–3533.

Garai, M., Sasmal, N., and Karmakar, B. (2015a). Effects of M2+ (M= Ca, Sr, and Ba) addition on crystallization and microstructure of SiO2-MgO-Al2O3-B2O3-K2O-F glass. *Indian J. Mater. Sci.*

Garai, M., Sasmal, N., Molla, A. R., and Karmakar, B. (2015b). Structural effects of Zn^{+2}/Mg^{+2} ratios on crystallization characteristics and microstructure of fluorophlogopite mica-containing glass-ceramics. *Solid State Sci.* 44, 10–21.

Garai, M., Sasmal, N., Molla, A. R., Singh, S. P., Tarafder, A., and Karmakar, B. (2014). Effects of nucleating agents on crystallization and microstructure of fluorophlogopite mica-containing glass–ceramics. *J. Mater. Sci.* 49, 1612–1623.

Garai, M., Sasmal, N., Molla, A. R., Tarafder, A., and Karmakar, B. (2015c). Effects of *in-situ* generated coinage nanometals on crystallization and microstructure of fluorophlogopite mica containing glass-ceramics. *J. Mater. Sci. Technol.* 31, 110–119.

Gautam, C., Yadav, A. K., and Singh, A. K. (2012). A review on infrared spectroscopy of borate glasses with effects of different additives. *ISRN Ceram.* 2012:428497.

Holand, W., Rheinberger, V., and Schweiger, M. (2001). Nucleation and crystallization phenomena in glass-ceramics. *Adv. Eng. Mater.* 3, 768–774.

Hubert, M., Faber, A. J., Akmaz, F., Sesigur, H., Alejandro, E., Maehara, T., et al. (2014). Stabilization of Divalent Chromium Cr(II) in Soda-lime-silicate Glasses. *J. Non Cryst. Solids* 403, 23–29.

Karamanov, A., Pisciella, P., and Pelino, M. (1999). The effect of Cr_2O_3 as a nucleating agent in iron-rich glass-ceramics. *J. Eur. Ceram. Soc.* 19, 2641–2645.

Kumar, V., Arora, A., Pandey, O. P., and Singh, K. (2008). Studies on thermal and optical properties of glasses as sealants for solid oxide fuel cells. *Int. J. Hydrogen Energy* 33, 434–438.

Laoot, P., Rangsriwatananon, K., and Chaisena, A. (2011). Synthesis of Sodium-type Fluorophlogopite Mica from Perlite and Diatomite. *J. Ceram. Process. Res.* 12, 273–278.

Lin, C., Liu, J., Han, L., Gui, H., Song, J., Li, C., et al. (2018). Study on the structure, thermal and optical properties in Cr_2O_3-incorporated MgO-Al_2O_3-SiO_2-B_2O_3 glass. *J. Non Cryst. Solids* 500, 235–242.

McDowell, J. F., and Beall, G. H. (1969). Immiscibility and Crystallization in $A1_2O_3$-SiO_2 Glasses. *J. Am. Ceram. Soc.* 52, 17–25.

Mcmillan, P. W. (1979). *Glass–Ceramics*. London: Academic Press.

Motke, S. G., Yawale, S. P., and Yawale, S. S. (2002). Infra-red spectra of zinc doped lead borate glasses. *Bull. Mater. Sci.* 25, 75–78.

Murata, T., Torisaka, M., Takebe, H., and Morinaga, K. (1997). Compositional dependence of the valence state of Cr ions in oxide glasses. *J. Non Cryst. Solids* 220, 139–146.

Nath, P., and Douglas, R. W. (1965). Cr^{3+}-Cr^{6+} equilibrium in binary alkali silicate glasses. *Phys. Chem. Glasses* 6:197.

Oliver, W. C., and Pharr, G. M. (1992). An improved technique for determining hardness and elastic modulus using load and displacement sensing indentation experiments. *J. Mater. Res.* 7, 1564–1583.

Pang, S., Zhang, T., Asami, K., and Inouse, A. (2002). Effects of Chromium on the Glass formation and corrosion behavior of bulk glassy Fe-Cr-Mo-C-B alloys. *Mater. Trans.* 43, 2137–2142.

Pingale, S. S., Patil, S. F., Vinod, M. P., Pathak, G., and Vijayamohanan, K. (1996). Mechanism of humidity sensing of Ti-doped MgCr2O4 ceramics. *Mater. Chem. Phys.* 46, 72–76.

Rezvani, M., Eftekhari-Yekta, B., Solati-Hashjin, M., and Marghussian, V. K. (2005). Effect of Cr_2O_3, Fe_2O_3 and TiO_2 Nucleants on the Crystallization

Behaviour of SiO_2-Al_2O_3-CaO-MgO (R_2O) Glass-ceramics. *Ceram. Int.* 31, 75–80.

Sasmal, N., Garai, M., and Karmakar, B. (2016). Influence of Ce, Nd, Sm and Gd oxides on the properties of alkaline-earth borosilicate glass sealant. *J. Asian Ceram. Soc.* 4, 29–38.

Shelby, J. E. (2005). "Principles of glass formation," in *Introduction to Glass Science and Technology*, eds M. Miller and P. Liaw (Cambridge: The Royal Society of Chemistry), 72–99.

Tarte, P. (1967). Infra-red Spectra of Inorganic Aluminates and Characteristics Vibrational Frequencies of AlO_4Tetrahedra and AlO_6Octahedra. *Spectrochim. Acta* 23A, 2127–2143.

Wu, X., Huang, S., Hommerich, U., Yen, W. M., Aitken, B. G., and Newhouse, M. (1995). Spectroscopy of Cr^{4+} in Mg-Ca-Ba aluminate glass. The coupling of $^3T_2$ and ^{1}E states. *Chem. Phys. Lett.* 233, 28–32.

Xiu, T., Liu, Q., and Wangab, J. (2006). Alkali-free borosilicate glasses with wormhole-like mesopores. *J. Mater. Chem.* 2006, 4022–4024.

Conflict of Interest: The authors declare that the research was conducted in the absence of any commercial or financial relationships that could be construed as a potential conflict of interest.